The Role of Background Cloud Microphysics in the Radiative Formation of Ship Tracks

S. PLATNICK,* P. A. DURKEE,+ K. NIELSEN,+ J. P. TAYLOR,# S.-C. TSAY,@ M. D. KING,@ R. J. FEREK,&,++ P. V. HOBBS,& AND J. W. ROTTMAN**

* *NASA Goddard Space Flight Center, Greenbelt, Maryland, and University of Maryland Baltimore County, Baltimore, Maryland*
+ *Department of Meteorology, Naval Postgraduate School, Monterey, California*
# *Meteorological Research Flight, The Met. Office, Farnborough, Hampshire, United Kingdom*
@ *NASA Goddard Space Flight Center, Greenbelt, Maryland*
& *Atmospheric Sciences Department, University of Washington, Seattle, Washington*
** *Science Applications International Corporation, San Diego, California*

(Manuscript received 27 June 1996, in final form 15 April 1997)

ABSTRACT

The authors investigate the extent to which the contrast brightness of ship tracks, that is, the relative change in observed solar reflectance, in visible and near-infrared imagery can be explained by the microphysics of the background cloud in which they form. The sensitivity of visible and near-infrared wavelengths for detecting reflectance changes in ship tracks is discussed, including the use of a modified cloud susceptibility parameter, termed the ''contrast susceptibility,'' for assessing the sensitivity of background cloud microphysics on potential track development. It is shown that the relative change in cloud reflectance for ship tracks is expected to be larger in the near-infrared than in the visible and that 3.7-μm channels, widely known to be useful for detecting tracks, have the greatest sensitivity. The usefulness of contrast susceptibility as a predictor of ship track contrast is tested with airborne and satellite remote sensing retrievals of background cloud parameters and track contrast. Retrievals are made with the high spatial resolution Moderate Resolution Imaging Spectroradiometer Airborne Simulator flown on the National Aeronautics and Space Administration's high-altitude ER-2 aircraft, and with the larger-scale perspective of the advanced very high resolution radiometer. Observed modifications in cloud droplet effective radius, optical thickness, liquid water path, contrast susceptibility, and reflectance contrast are presented for several ship tracks formed in background clouds with both small and large droplet sizes. The remote sensing results are augmented with in situ measurements of cloud microphysics that provide data at the smaller spatial scales.

1. Introduction

Ship tracks have provided intriguing examples of cloud albedo modification by anthropogenic aerosols since their discovery with early satellites by Conover (1966) and their proposed explanation by Conover (1966, 1969) and Twomey et al. (1968). Discussion of a possible climatic consequence to large-scale aerosol pollution modification of cloud albedo by Twomey (1974, 1977) gave the ship track phenomena considerable attention in cloud–climate interaction studies (e.g., Charlson et al. 1992). Though ship tracks certainly provide a possible microcosm for this so-called indirect effect of aerosols on climate, their interest in this paper is from a local perspective only. Ship tracks are interesting in their own right, in addition to providing one of the best instances of a ''controlled experiment'' for use in cloud microphysical and radiative studies. That is, a track can reasonably be expected to develop in conditions identical to the background cloud in which it forms, except for modification to a single input—the aerosol amount.

The Monterey Area Ship Track (MAST) experiment provided a unique opportunity for the remote sensing of ship tracks and the background marine stratocumulus in which they form. First, using imagery and in situ data acquired during the MAST experiment, this paper explores the extent to which the detection of ship tracks in multispectral imagery can be explained by parameters of the background clouds. These parameters include liquid water content, droplet size, and optical thickness. Second, we ask whether the relative brightness of ship tracks can be correlated with the background cloud parameters. That is, to what extent can the radiative

++ Current affiliation: Office of Naval Research, Washington, D.C.

Corresponding author address: Dr. Steven Platnick, Code 913, NASA Goddard Space Flight Center, Greenbelt, MD 20771.
E-mail: platnick@climate.gsfc.nasa.gov

strength, or contrast, of observed tracks be predicted from the microphysics and optical thickness of the surrounding clouds. With this terminology, detection is determined by the minimum contrast that can be observed by a remote instrument. The following sections explore the implications of track detection and track contrast, either of which is considered an aspect of ship track radiative formation. A modification to the cloud susceptibility parameter (Twomey 1991), dubbed the ''contrast susceptibility,'' is invoked as a useful sensitivity parameter for track formation.

In addition to background cloud conditions, the increase in cloud droplet numbers caused by a ship plays a fundamental role in track brightness. This will be discussed in more detail later. There are also meteorological conditions that must be met for the development of tracks (Coakley et al. 2000). Further, ship-induced boundary layer perturbations might affect the initial track development (G. E. Innis et al. 1997, unpublished manuscript). These dynamic influences are the subject of other papers in this special issue. In the following discussions, we deal only with the cloud microphysical component.

The cloud parameters needed for the analysis are primarily obtained with remote sensing cloud algorithms applied to multispectral imagery, though some in situ measurements are also used. Cloud droplet size, optical thickness, and liquid water path are inferred from solar reflection measurements in the visible and near-infrared that are nonabsorbing and absorbing, respectively, for cloud droplets. As a simplification, the visible reflectance contains the optical thickness information, while the near-infrared reflectance indicates particle size since fractional droplet absorption is approximately proportional to droplet radius. The typical absorbing channels, dictated by the atmospheric transmittance windows, are in the 1.6-, 2.1-, and 3.7-μm bands. The 3.7-μm band poses some difficulty in that cloud emission is a significant part of the total measured radiance and must be accounted for.

This study uses two imaging radiometers: the Moderate Resolution Imaging Spectroradiometer (MODIS) Airborne Simulator (MAS) flown on the National Aeronautics and Space Administration's high-altitude ER-2 aircraft (King et al. 1996), and the advanced very high resolution radiometer (AVHRR) aboard the National Oceanic and Atmospheric Administration (NOAA) polar-orbiting satellites. The MAS contains spectral channels in all the visible and near-infrared bands useful for cloud remote sensing. On the AVHRR, the sole droplet absorption channel for solar radiation is at 3.7 μm. At nominal ER-2 altitudes of 20 km, the MAS nadir resolution for marine boundary layer clouds is 50 m with a swath width of 35 km. The high spatial resolution offers an unprecedented view of ship track structure. The ER-2 made seven flights during MAST, and ship tracks were found in MAS imagery on three of the flight days. Microphysical retrievals derived from the MAS have been compared with University of Washington C-131A in situ measurements on days both with and without tracks. These comparisons are discussed in section 3a. AVHRR 1-km data were acquired by the Naval Postgraduate School in Monterey, California. While having much less spatial resolution than the MAS, AVHRR instruments provided multiple daily passes of the MAST operations area and are capable of larger-scale studies with their 2400-km swath width. This paper looks at track retrievals from six morning passes of *NOAA-12*. The U.K. Meteorological Research Flight C-130 aircraft provided in situ droplet radius and above-cloud reflectance measurements, providing the highest spatial resolution but with limited spatial sampling. Measurements from all platforms are used for developing the ship track microphysical statistics needed for assessing the correlation between contrast susceptibility and track contrast.

Section 2 begins with a review of the physics behind the reflectance increases, both visible and near-infrared, observed in ship track imagery. The sensitivity of relative reflectance changes to modification in droplet numbers is discussed in terms of a cloud susceptibility parameter. It is shown that the sensitivity increases with increasing droplet absorption, or wavelength, with the 3.7-μm band being most sensitive, typically several factors greater than for the visible. Section 3 presents results of MAS and AVHRR retrievals, including statistics of droplet size, optical thickness, and liquid water path changes. Finally, the utility of using background cloud microphysics in predicting ship track brightness with 3.7-μm contrast susceptibilities is discussed in section 4.

2. The reflectance contrast of ship tracks in visible and near-infrared imagery

a. Cloud reflectance in the visible and near-infrared

The reflectance of solar radiation from clouds depends on a combination of the cloud optical thickness, τ; cloud droplet single scattering albedo, ϖ_0; and droplet scattering phase function. For a given set of microphysical conditions, optical thickness has a wavelength dependence through the droplet extinction efficiency. The single scattering albedo is the fraction of incident energy scattered by a droplet, and so fractional absorption is given by $1 - \varpi_0$. Absorption by liquid water is negligible in the visible and $\varpi_0 = 1$. In the near-infrared, fractional droplet absorption is significant and approximately proportional to the product of droplet radius and water bulk absorption at the wavelength of interest (Twomey and Bohren 1980; Stephens and Tsay 1990). Consequently, for a given optical thickness, clouds with larger droplets reflect less near-infrared energy. This has significant implications for ship track observations and the remote sensing of droplet sizes. For multiple scattering situations, such as the clouds of this study, the effect of the phase function can often be described by

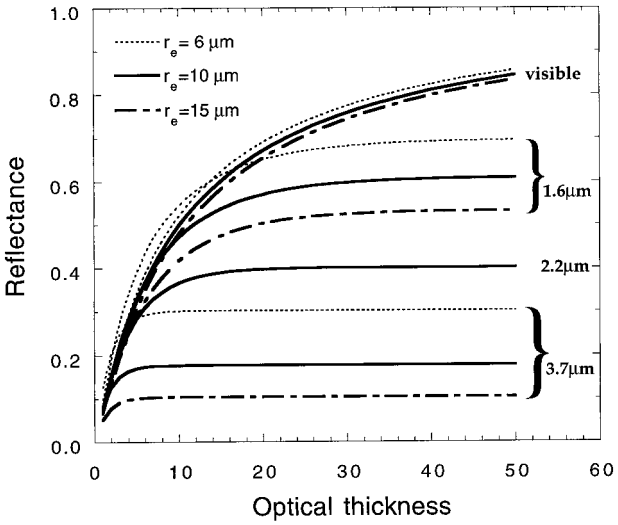

FIG. 1. Plots of bidirectional reflectance vs optical thickness for the MODIS Airborne Simulator channels with central wavelengths at 0.65, 1.62, 2.13, and 3.74 μm. Reflectance for each channel is shown for cloud droplet effective radii of 6, 10, and 15 μm (or only a 10-μm radius for the 2.13-μm channel). Calculations are averaged over the azimuth, where the cosine of the solar and satellite viewing angles are 0.65 and 0.85, respectively. Optical thickness is the visible equivalent.

the asymmetry parameter, g, a scalar indicating the amount of scattered energy directed into the forward direction ($g = 0$ for isotropic scattering and varies from about 0.75 to 0.9 for cloud droplets in the visible and near-infrared). As with single scattering albedo, the asymmetry parameter also depends on droplet size and wavelength. In general, larger droplets have greater asymmetry parameters and exhibit more forward scattering. With more forward scattering there is less chance of incoming photons being turned around, and cloud reflectance decreases.

For a distribution of droplet sizes, as occurs in clouds, the droplet effective radius, r_e, is the pertinent radiative transfer size parameter (defined as $\langle r^3\rangle/\langle r^2\rangle$). We can therefore write the functional dependence of reflectance as $R = R_\lambda(\tau, \varpi_0, g) = R_\lambda(\tau, r_e)$ where the wavelength dependence is indicated. These concepts are summarized in Fig. 1, which shows the calculated reflectance for a plane-parallel cloud as a function of optical thickness (scaled to the visible value). Up to this point, we have used the term cloud reflectance generically to describe upwardly scattered radiation. More precisely, cloud albedo is the fraction of incident energy scattered back into the upward hemisphere. Figure 1 shows the bidirectional reflectance, which is the albedo inferred from some particular viewing direction if the scattered radiance is assumed isotropic. The curves of Fig. 1 cover the visible and near-infrared bands used in the MAS and AVHRR instruments at three different effective radii. In the near-infrared bands, liquid water absorption increases with increasing wavelength, and so reflectance curves for the same droplet size are seen to decrease significantly at the longer wavelengths. Likewise, for a fixed band, near-infrared reflectance decreases with increasing droplet sizes as absorption increases. This reflectance is seen to approach an asymptotic limit as optical thickness increases to a point where photons can no longer survive the many scatterings it takes to reach the bottom of the cloud and then return to cloud top. In the visible, it is the relatively small effect of the asymmetry parameter that accounts for the slight decrease in reflectance for the larger droplets.

Both increases in optical thickness and decreases in droplet size are expected in ship tracks. For a fixed droplet size, cloud reflectance will increase with optical thickness, though with diminishing importance into the near-infrared because of droplet absorption. For a fixed cloud optical thickness in the near-infrared, both absorption and forward scattering decrease with decreasing droplet size, and so reflectance also increases; of the two influences, absorption dominates the scattering effect. From a remote sensing standpoint, it is clear that reflection measurements in both the visible and near-infrared contain information about both optical thickness and droplet effective radius. The most unambiguous information occurs when the near-infrared reflectance has reached its asymptotic value and is no longer dependent on the retrieval of optical thickness. For present purposes, it is also clear that changes in cloud droplet sizes can be observed as changes in near-infrared reflectance.

b. Visible and near-infrared cloud susceptibilities

For the purposes of this study, a track is said to exist when a detectable increase in reflectance is observed. Detectability means that the relative change in the bidirectional reflectance, that is, $\Delta R/R$, or ''track contrast,'' is larger than instrument noise and existing cloud variability. Because of these dependencies, absolute detectability is not as meaningful as the relative detectability among various visible and near-infrared bands. Once a ship track is detected, the observed value of $\Delta R/R$ is a measure of its radiative strength. Track detectability and observed contrast are considered two aspects of track formation. The influence of background cloud parameters on ship track radiative formation then becomes a measure of its influence on detectability and the potential value of $\Delta R/R$. We begin this section by exploring the relative sensitivity of visible and near-infrared imagery for ship track detection. Further, we will demonstrate that 3.7-μm reflected sunlight is likely to be a much more sensitive method for detecting microphysical changes than current in situ instrumentation. We close the section with a discussion of ship track contrast.

Ships are believed to modify droplet concentrations, N, by adding cloud condensation nuclei to a developing or existing cloud (Conover 1966; Twomey et al. 1968).

This hypothesis is supported by the MAST studies described in this special issue. One measure for the sensitivity of cloud albedo to changes in cloud droplet concentration is dA/dN, which has been defined as ''cloud susceptibility'' (Twomey 1991; Platnick and Twomey 1994), where A is cloud albedo. Intended as a sensitivity parameter for indicating the potential indirect effect of aerosol on climate, susceptibility can also be used for present purposes with slight modification. In the context of this paper, an indicator of potential ship track formation would be $(dR/R)/dN$, where the relative change in bidirectional reflectance is the quantity of interest. This can be termed a contrast susceptibility to distinguish it from the original definition of cloud susceptibility. As a sensitivity parameter, contrast susceptibility can be used to gauge the likelihood of detection. Unless noted, further use of the term susceptibility will refer to the contrast formulation. Recalling that reflectance for a particular band has the functional dependence $R(\tau, r_e)$, contrast susceptibility can be written as

$$\frac{1}{R}\frac{dR}{dN} = \frac{1}{R}\left(\frac{\partial R}{\partial r_e}\frac{dr_e}{dN} + \frac{\partial R}{\partial \tau}\frac{d\tau}{dN}\right), \tag{1}$$

where the wavelength dependence is understood. With the assumption that the liquid water content, W, in a track remains the same as in the background cloud, ship track optical thickness would be expected to increase above the background value by $N^{1/3}$ and droplet sizes would decrease as $N^{-1/3}$. Ferek et al. (1998, 2000) found that liquid water content measured in a number of ship tracks was not, on average, significantly increased compared with the background cloud as was suggested by the track measurements of Radke et al. (1989). For a constant liquid water process, contrast susceptibility can be written as

$$\frac{1}{R}\frac{dR}{dN} = \frac{1}{R}\frac{C}{W}\left(-\frac{\partial R}{\partial r_e}r_e^4 + \tau\frac{\partial R}{\partial \tau}r_e^3\right), \tag{2}$$

where the constant $C = 4\pi\rho_l/9$ with ρ_l as the density of liquid water. In the visible, the second term in parentheses dominates, while for the 3.7-μm band, the second term vanishes at larger thicknesses (cf. Fig. 1). Note that $\partial R/\partial r_e$ is a negative quantity ensuring that near-infrared reflectance increases with droplet concentration. A detailed derivation of Eq. (2) is not given as it closely follows the development of cloud susceptibility in Platnick and Twomey (1994), including assumptions regarding the relationship between various moments of the droplet size distribution (see also Taylor and McHaffie 1994). Figure 2a shows contrast susceptibility calculated as a function of effective radius in visible and near-infrared bands for an optical thickness of 20. It is seen that the susceptibility increases with the longer wavelengths as the droplet absorption effect dominates. Figure 2b gives the ratio of the 3.7-μm contrast susceptibility to the visible for a range of optical thicknesses. The sensitivity in the 3.7-μm band is seen to be a factor of 2 to 8 greater than in the visible for the prescribed geometry.

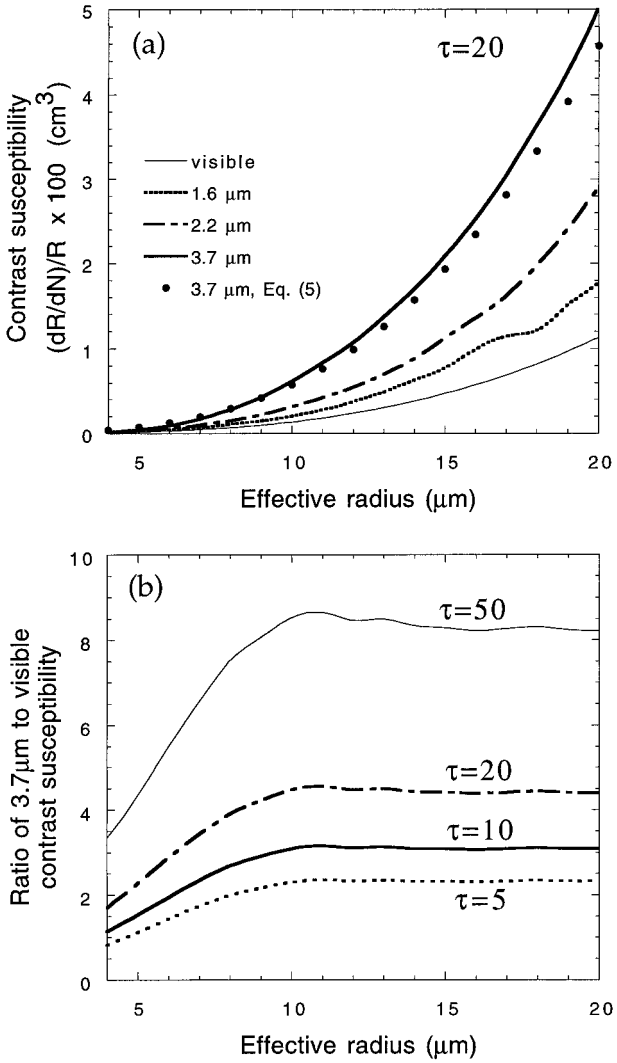

FIG. 2. (a) The contrast, or relative, susceptibility calculated in visible and near-infrared bands as a function of cloud droplet effective radius for an optical thickness of 20 (visible equivalent). An empirical approximation for the 3.7-μm curve is also shown (see text). (b) Ratios of the 3.7-μm contrast susceptibility to the visible for a wide range of optical thicknesses. Solar and viewing geometries are the same as in Fig. 1; liquid water content is 0.3 g m^{-3}.

The partial derivatives in this study are determined from adding/doubling reflectance calculations (Twomey et al. 1966). However, simple approximations are useful for instructive purposes. For example, neglecting the droplet size dependence of the asymmetry parameter, two-stream approximations for the visible reflectance (Bohren 1987) can be used to write $\tau\partial R/\partial\tau$ in the second term of Eq. (2) as $R(1 - R)$, giving the optical thickness dependence of the equation as

$$\frac{1}{R_{\text{vis}}}\frac{dR_{\text{vis}}}{dN} \approx \frac{C}{W}(1 - R_{\text{vis}})r_e^3. \tag{3}$$

The two-stream formulas work well for visible reflectance, but susceptibilities from Eq. (3) are about 30%–40% higher than the visible curve of Fig. 2a. Equation (3) can also be written in terms of cloud optical thickness with $1 - R_{\text{vis}} \approx 2/[2 + (1 - g)\tau]$.

Two-stream approximations for absorbing wavelengths are more difficult to manipulate. Reflectance for an optically thick cloud layer can be approximated as $(\sqrt{1 - \varpi_0 g} - \sqrt{1 - \varpi_0})/(\sqrt{1 - \varpi_0 g} + \sqrt{1 - \varpi_0})$ (Bohren 1987). After approximating single scattering albedo with $\varpi_0 \approx 1 - 0.85kr_e$ (Twomey and Bohren 1980), where k is the bulk absorption coefficient of water at the wavelength of interest, a power series expansion in terms of effective radius was derived for near-infrared contrast susceptibility in the optically thick limit. Ignoring the size dependence of g, the first term in the expansion is

$$\frac{1}{R_{\text{nir}}}\frac{dR_{\text{nir}}}{dN} \approx \frac{C}{W}\left(\frac{0.85k}{1 - g}\right)^{1/2} r_e^{7/2}. \tag{4}$$

This approximation gives near-infrared susceptibilities about 15%–40% less than those shown in Fig. 2a but with the correct characteristic shape. As a more accurate alternative for the 3.7-μm band, a fitting routine applied to Fig. 1 for effective radii between 5 and 20 μm and a wide range of solar angles gives $R_{3.7} \approx 2.9r_e^{-1.2}$ for a thick cloud with r_e in micrometers. If a power law can adequately describe reflectance, then, regardless of the value of the exponent, $R_{3.7}^{-1}(\partial R_{3.7}/\partial r_e) \propto r_e^{-1}$. Substitution into Eq. (2) leads to

$$\frac{1}{R_{3.7}}\frac{dR_{3.7}}{dN} \approx \frac{C}{W}1.2r_e^3, \tag{5}$$

giving 3.7-μm susceptibilities within 10% of Fig. 2a. For example, with $W = 0.3$ g m^{-3}, Eq. (5) becomes $5.7 \times 10^{-6}\, r_e^3$, with r_e in micrometers and contrast susceptibility in cm^3. Then if $r_e = 12$ μm, the susceptibility would be about 0.01 cm^3, implying that a 3.7-μm channel contrast of 1% would result from an increase in droplet concentration of only 1 cm^{-3}. The ratio of the 3.7 μm to visible susceptibility is now approximated as simply $1.2/(1 - R_{\text{vis}})$, which is constant for any prescribed optical thickness (or R_{vis}). For the larger effective radii, this approximation is about 30% less than the curves of Fig. 2b due to the overestimation of visible susceptibility. All calculations of susceptibility in the following sections use a nominal liquid water content of 0.3 g m^{-3}, which is typical of these stratocumulus clouds (e.g., Noonkester 1984).

Figure 2 indicates that from radiative considerations alone, ship tracks are expected to be more easily observed in near-infrared channels than in the visible, and that the 3.7-μm channel has the most sensitivity [as noticed in the observations of Scorer (1987); Coakley et al. (1987)]. Though the plots of Fig. 2 are for differential changes in droplet numbers, finite differences are fairly well approximated by the same curves. An example of contrast is seen in the four-channel MAS images of Fig. 3 for two tracks, both of which formed in relatively clean background conditions. The unidentified track from 13 June is seen to be formed by a container ship in 6-m resolution photography taken with the ER-2 Wild-Heerbrugg RC-10 camera. This MAS image covers a region of 11 km (in the horizontal or scan direction) by 24 km (in the vertical). The diesel-powered *Star Livorno* was identified as having formed the track on 29 June in the lower image, which covers a region of 35 km (the full MAS scan direction) by 43 km. The images have not been spatially resampled across the scan line so pixels near the edges comprise larger areas than those at nadir (more important for the lower image). Retrievals for these tracks are discussed in the next section. For now we note that the apparent track contrast is more obvious as wavelength increases. For the relatively high sun angles in these images (cosine of the solar zenith angle, μ_0, about 0.95), track contrast in the 3.7-μm channel is expected to be about a factor of 1.6 greater than that for the visible channel. AVHRR images have lower sun angles at these latitudes during the satellite overpass times and should show more dramatic contrast differences as indicated by Fig. 2b where $\mu_0 = 0.65$. In addition to the contrast depending on wavelength, it is also seen that the background variability in the visible image of 29 June helps to obscure the track and reduce contrast. The effect of optical thickness variability on visible track contrast was discussed by Coakley et al. (1987). However, it is not clear that background variability fully explains the limited track seen in this particular visible image. Another possibility may be heterogeneous cloud effects, which could be more pronounced at less absorbing wavelengths.

We now discuss the ability of a 3.7-μm channel for detecting finite microphysical changes. Figure 4 shows the 3.7-μm relative reflectance change that accompanies a given decrease in track effective radius. Note that sub micron changes in droplet sizes should be easily observed. For example, a relative reflectance increase of 5%, which should be obvious in most sensors for correspondingly small background variability, would indicate a reduction in droplet size of only 0.5 μm. Such sensitivity is likely to be larger than that from commonly available in situ instruments such as the Forward Scattering Spectrometer Probe (FSSP) with its several micrometer droplet size bins (Knollenberg 1981), especially against the natural variability seen in aircraft data (Ferek et al. 2000). However, since 3.7-μm imagery includes a significant thermal component, it should be noted that a relative reflectance increase of 5% would mean a smaller increase in the total measured channel radiance, or intensity, I_m, which is the sum of the reflected and emitted radiance and is a function of droplet size, cloud temperature, and geometry. The measured radiance can be written as $I_m \approx Rt(\mu)t(\mu_0)\mu_0 F_0/\pi + (1 - R)B(T_c)t(\mu)$, where μ and μ_0 represent the cosine

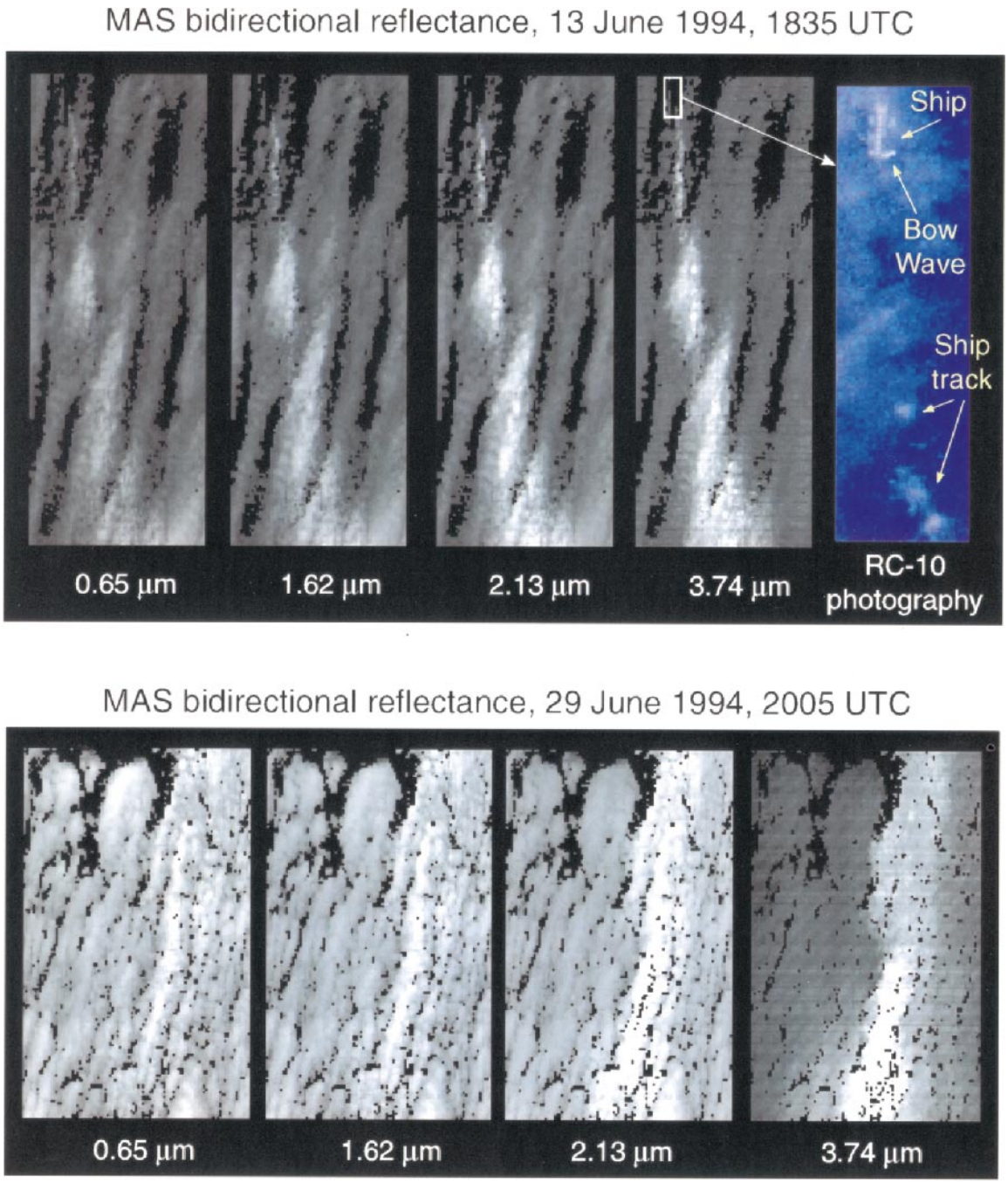

FIG. 3. Cloud reflectance in four visible and near-infrared MODIS Airborne Simulator channels showing the general increase in ship track contrast at the longer wavelengths. The unidentified track from 13 Jun was photographed with the RC-10 camera on board the ER-2 and found to be a container ship. The diesel-powered *Star Livorno* was identified as having formed the track from 29 Jun. The sizes of the imaged areas are given in the text. Model calculations suggest that at the relatively high sun angles present during these flights, the 3.7-μm track contrast would be about a factor of 1.6 greater than in the visible; larger contrast differences would be expected at lower sun angles. Emission has been removed from the 3.7-μm channel.

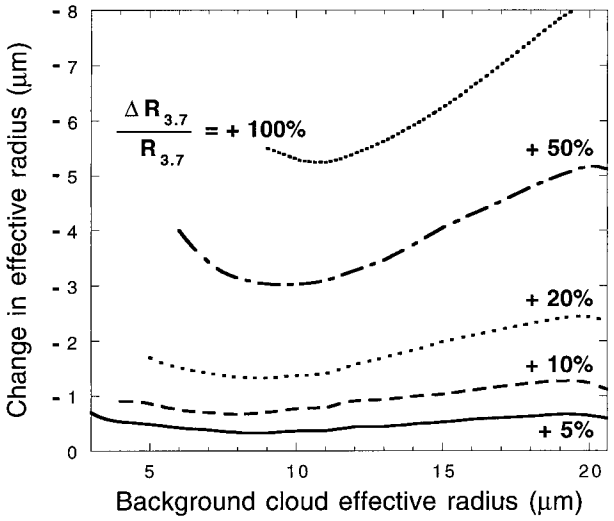

FIG. 4. Curves showing the relative change (in percent) in 3.7-μm cloud reflectance expected for a given reduction in droplet size occurring in a ship track relative to the background cloud in which it forms. Solar and viewing geometries are the same as in Fig. 1; liquid water content is 0.3 g m^{-3}.

of the viewing and solar zenith angles, respectively; $B(T_c)$ is the Planck function evaluated at the cloud temperature; F_0 is the solar flux in the 3.7-μm band; t is the transmittance between cloud top and the top of the atmosphere; and emissivity in the viewing direction has been approximated as being $1 - R$. The relative change in solar reflectance can then be approximated as

$$\frac{\Delta R}{R} \approx \frac{\Delta I_m}{I_m} \frac{1}{1 - \dfrac{B(T_c)t(\mu)}{I_m}}. \tag{6}$$

Radiative transfer calculations show that the second term on the right-hand side can be approximated as a linear function of effective radius, with slope primarily dependent on cloud temperature and μ_0, and the atmospheric transmittance having secondary importance for the marine boundary layer clouds of this study. For example, with a cloud-top temperature of 285 K and $\mu_0 = 0.65$, the second term is approximated as $0.8 + 0.09r_e$, with r_e in micrometers. Using this approximation, a 5% increase in relative reflectance would correspond to an increase in measured radiance of about 3% for an effective radius of 10 μm, still within sensor capability. The approximation ranges from $0.90 + 0.38r_e$ to $0.8 + 0.11r_e$ for $T_c = 275$ K, $\mu_0 = 0.95$ and $T_c = 290$ K, $\mu_0 = 0.65$, respectively.

The above discussion focused mainly on the detectability of ship tracks in multiwavelength imagery. A second goal of this paper is to understand the role of cloud microphysics in the observed contrast of ship tracks. In addition to knowledge of the background cloud droplet size, optical thickness, and liquid water content (collectively represented by the contrast susceptibility parameter), a prediction of droplet concentration changes, ΔN, is needed to infer ship track contrast. For small changes in either ΔN or $\Delta N/N$, track contrast is approximately the product of contrast susceptibility and the droplet concentration change. Figure 5a shows plots of track contrast versus susceptibility for a wide range of ΔN. Figure 5b shows the same plot versus effective radius, where the r_e^3 dependence of susceptibility is seen. A liquid water content of 0.3 g m^{-3} is used in the calculations, and solar and viewing angles are the same as in Fig. 1. Smaller liquid water contents will shift the curves to the right, such that a given susceptibility will correspond to a smaller contrast for the same ΔN. There is some angular dependence as well. Figure 5 *is* the role of background cloud microphysics in the radiative formation of ship tracks—the abscissa

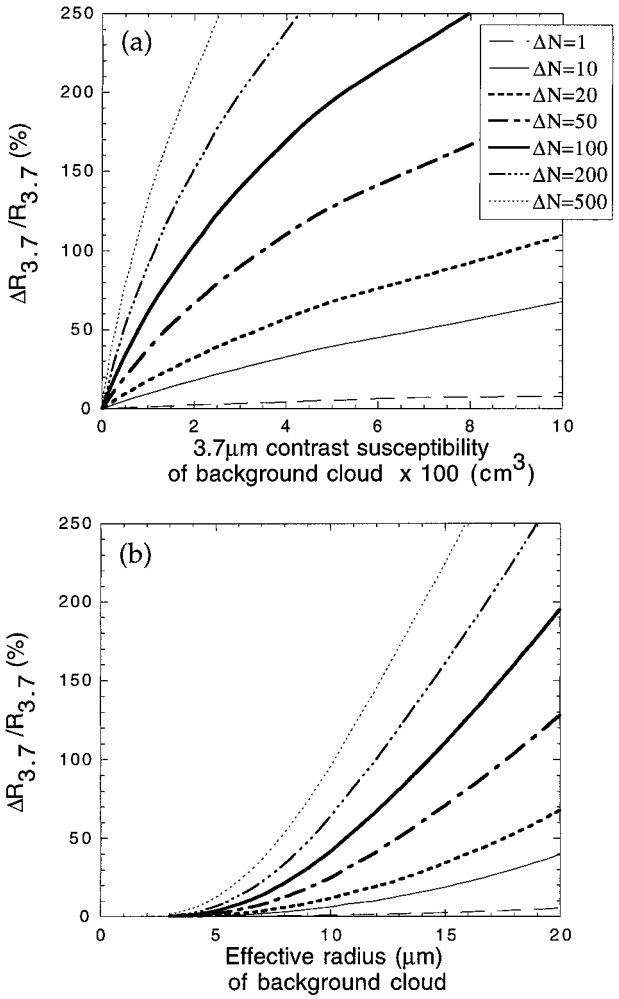

FIG. 5. (a) Calculations showing the ship track contrast in the 3.7-μm band vs the contrast susceptibility of the background cloud for a wide range of droplet concentration increases (ΔN). Calculated for a liquid water content of 0.3 g m^{-3}, an optical thickness of 10, and with solar and viewing angles the same as for Fig. 1. (b) The same as in (a) but with the abscissa transformed to effective droplet radius.

parameterizes microphysics and the ordinate is the measure of formation.

The range of observed ΔN in actual ship tracks is important in determining the extent to which a set of curves like those in Fig. 5 is useful for approximating ship track contrast from susceptibility alone. Two possibilities come to mind. First, if measured droplet increases are typically found to be within some bound, then such empirical information could be used to determine the uncertainty in inferring track contrast from Fig. 5. For instance, though aerosol and cloud condensation nuclei numbers may be very large in tracks, droplet numbers typically show a more moderate range of increases. Droplet increases measured by the University of Washington C-131A (Hobbs et al. 2000) ranged from about 50 to 200 cm^{-3} in four different tracks produced by diesel-powered ships. Second, if droplet increase is found to depend to some extent on background cloud microphysics, which is described by susceptibility, then the broad range in track contrast covered by the multiple curves of Fig. 5 should be reduced. Other results from the MAST experiment should be helpful in resolving this issue.

Contrast susceptibility represents the radiative role of microphysics in ship track formation. A simple cloud model has been used for predicting susceptibility by assuming conserved liquid water content and a single-layer cloud with vertical and horizontal homogeneity. It is not expected that such a model will always be successful in describing the radiative signature of ship tracks, especially when more complex stratocumulus cloud fields develop.

3. Remote sensing results

We have discussed the influence of background cloud microphysics on the reflectance contrast of a ship track, particularly in a 3.7-μm band, by introducing the contrast susceptibility parameter. This parameter is primarily a function of cloud droplet effective radius which can be retrieved through solar reflection measurements. Likewise, because of emission, the reflectance contrast of a ship track in a 3.7-μm channel can be determined from the observed contrast in total radiance only after the cloud effective radius is known [see Eq. (6)]. In this section we retrieve effective radius in the vicinity of ship tracks using both the MAS and the AVHRR instruments. Subsequent calculations of the contrast susceptibility and track contrast are presented in section 4 where correlations are plotted in a manner similar to Fig. 5.

As previously discussed, a combination of visible (nonabsorbing) and near-infrared (absorbing) channels are used to retrieve cloud optical thickness and effective radius. The MAS and AVHRR retrieval algorithm for using the 3.7-μm band as the absorbing channel, which is accompanied by significant emission, is based on Platnick and Valero (1995). Channel emission is removed with an estimate of cloud-top temperature from a thermal infrared channel. MAS retrievals using shorter wavelength near-infrared channels at 1.6 and 2.1 μm, with less absorption and no emission, are special (simpler) cases of the algorithm. The correlated *k*-distribution technique of Kratz (1995) is used to calculate atmospheric transmission and/or emission for all MAS and AVHRR channels. Atmospheric water vapor and temperature profiles needed for the calculations are taken from sondes released from the ship *Glorita* during MAST (Syrett 1994).

a. MODIS Airborne Simulator retrievals

Though the current MAS data system (King et al. 1996) allows for the recording of 50 channels from the visible through the thermal infrared, the system was limited to 11 spectral channels during the MAST experiment in June 1994. Channels were chosen in those bands most useful for cloud remote sensing. Central wavelengths of channels selected for the MAST configuration include those at 0.65, 0.87, 1.62, 1.89, 2.13, 3.74, and 11.02 μm.

Absolute radiometric calibration of the MAS solar channels are made in the laboratory with an integrating sphere that is calibrated against a standard lamp (Arnold et al. 1996; King et al. 1996). Relative changes in calibration are monitored with a smaller, portable source placed beneath the MAS prior to each flight. At the time of the MAST deployment, the MAS in-flight temperature was unregulated. A relationship between the room temperature laboratory calibration and the calibration valid at cooler in-flight temperatures was derived from thermal-vacuum chamber tests. This gave a 7%–10% correction to 1.62- and 2.13-μm channels, while visible channels were unaffected. The total uncertainty in the temperature-corrected radiometric calibration of these channels during the MAST experiment, including laboratory calibrations, is difficult to resolve. However, it should be noted that even a $\pm$5% uncertainty in measured reflectance corresponds to an uncertainty in retrieved droplet sizes of about $\pm$15% and $\pm$10% in the 1.62- and 2.13-μm channels, respectively; doubling the reflectance uncertainty to $\pm$10% roughly doubles the size uncertainty to $\pm$30% and $\pm$20%, respectively. Comparisons of MAS reflectances with other ER-2 sensors is ongoing (Arnold et al. 1996). Recent modifications to the MAS have included heating elements, insulation, and airflow barriers. The 3.7-μm and thermal channels are calibrated in flight with two onboard blackbody panels, at ambient (cold) and warm temperatures, with empirical emissivity corrections (Moeller et al. 1996). The 3.7-μm retrieval is less sensitive to reflectance errors, with a $\pm$10% uncertainty in the inferred reflectance roughly corresponding to an equivalent $\pm$10% uncertainty in retrieval size (see Platnick and Valero 1995).

Seven ER-2 flights were made during MAST covering

a region as far as 500 km off the coast of Monterey Bay. Flight plans typically involved offset parallel runs to map out large regions and increase the chances of overflying a track. For logistical reasons, flights were flown around midday. Results of MAS ship track retrievals follow a discussion of MAS effective radius retrievals.

1) COMPARISONS OF MAS RETRIEVALS WITH IN SITU MEASUREMENTS

Effective radius retrievals are used for calculating both cloud contrast susceptibility and ship track contrast in the 3.7-μm channels. Therefore, the relative accuracy of these retrievals is of interest. Validation of satellite and airborne retrievals with in situ measurements, though long recognized as an important issue (e.g., Twomey and Cocks 1989; Rawlins and Foot 1990; Nakajima et al. 1991), is a difficult endeavor and beyond the scope of this paper. Here, we only summarize results of some comparisons made during MAST. The consequence of size retrieval errors on track contrast and contrast susceptibility calculations (i.e., the location of points on Fig. 5) will be delayed until section 4.

Comparisons between MAS effective radius retrievals and University of Washington C-131A in situ measurements were made during coordinated flights between the C-131A and the ER-2. The C-131A underflew the MAS during five of the seven ER-2 flights. Of those five flights, four occurred in regions of relatively uniform stratus suitable for validation studies. These flights were on 11, 28, 29, and 30 June 1994; the times of the coordinations were 1800–1900, 1700–1850, 1910–1940, and 2000–2100 UTC, respectively. During most of that time the C-131A was flying at a constant altitude, normally in the middle to upper part of the cloud. In situ droplet effective radii were measured with the Particle Measuring Systems' FSSP-100 and corrected for coincidence and dead time losses (Baumgardner 1982; Mossop 1983). Constant-altitude FSSP measurements showed relatively small droplet sizes, of about 7 μm, on all days except 29 June when average in situ effective radii measured about 13 μm. There was a large variability seen in the FSSP effective radius measurements during the constant-altitude flights, typically of about $\pm$1–2 μm, but as high as $\pm$4 μm on 29 June. No coordinated flights occurred across a ship track.

Adequate statistical knowledge of the cloud microphysical profile is important since marine stratocumulus boundary layer clouds are known to have measurable increases of both droplet sizes and liquid water content with height (e.g., Noonkester 1984; Garrett and Hobbs 1995). With typical droplet size increases of 50%–100%, there is no single in situ size measurement that can be simply equated with the retrieved effective radius. Rather, near-infrared retrievals will constitute some vertical weighting of droplet sizes in the cloud (Nakajima and King 1990; Platnick 1997). Weaker droplet absorption gives greater weighting to droplet sizes farther down in the cloud, so the more absorbing 3.7-μm band has the least vertical penetration and therefore the larger expected retrieved sizes. A calculation of the expected size retrieval with each near-infrared channel can be made if the profile is known. However, FSSP measurements of droplet size through the vertical extent of the cloud were usually only available from a single profile, giving few data points away from the constant-altitude position. It is doubtful that these few measurement points are statistically significant given the horizontal variability already mentioned. In the absence of sufficient vertical sampling, and with the constraint that cloud droplet number concentrations are constant with height, two extreme cases were used to specify an effective radius profile from the FSSP measurements: 1) an adiabatic profile where liquid water content is linear with height (i.e., LWC $\sim z$ implying $r_e \sim (\tau_c - \tau)^{1/5}$, where z is vertical height in the cloud, τ is the optical depth coordinate measured from cloud top down, and τ_c is the total cloud optical thickness), and 2) a substantially subadiabatic profile where effective radius is linear with optical depth ($r_e \sim \tau_c - \tau$ implying LWC $\sim$ (constant $- z)^{-3}$. Cloud-top and cloud-base FSSP measurements, though sparse, were used to set the boundary conditions for the profiles.

Using the two profiles, theoretical calculations for the expected range of retrieved effective radius (typically a 2–3-μm range) were compared with MAS retrievals for the four days. The retrievals were made using a visible channel in combination with each of the three near-infrared channels, and typically sampled more than 10 000 pixels covering a region of over 1000 km^2. The 1.6-μm retrievals are on average slightly less than retrievals from the 2.1-μm channel ($<$1 μm) as expected, though both are about 15%–20% less than the mean size expected from FSSP derived profiles. Though still consistent with calibration uncertainties as previously discussed, this is opposite to the overestimation of size usually seen in these wavelengths (Twomey and Cocks 1989; Rawlins and Foot 1990; Nakajima et al. 1991). The 3.7-μm retrievals of effective radius are about 20%–40% larger than expected. While this discrepancy may indicate error in MAS calibration or in the physical theory (including cloud radiative model, thermal corrections, and atmospheric transmittances), accuracy of the in situ measurements must also be considered. For example, effective radii measured with the PVM-100A (Gerber et al. 1994) were found to be about 50% higher than the FSSP; both operated simultaneously on the University of Washington C-131A in marine stratocumulus in the mid-Atlantic. A concurrent validation study using the same two in situ instruments and the AVHRR 3.7-μm channel showed retrievals averaging about 15% greater than the FSSP over a large-scale region (Platnick and Valero 1995). If effective radii were greater than FSSP inferences, then the overestimation in 3.7-μm re-

trievals would decrease, but the underestimation in 1.6- and 2.1-μm retrievals would increase.

In summary, a significant discrepancy exists between MAS 1.6- and 2.1-μm retrievals and 3.7-μm retrievals, though absolute errors are difficult to determine. However, effective radius retrievals, using any one of the near-infrared channels, give droplet sizes that differ with those expected from FSSP measurements by a nearly constant relative amount. That is, the ratio of MAS size retrievals to those derived from the FSSP are approximately constant. This relative difference allows simple approximations to be made for the effect of retrieval errors on subsequent calculations of 3.7-μm susceptibility and contrast (see section 4). A discussion of error sources and validations for the AVHRR 3.7-μm channel can be found in Platnick and Valero (1995), Nakajima and Nakajima (1995), and Han et al. (1995).

2) MAS RETRIEVALS OF SHIP TRACKS

Ship tracks were observed in MAS imagery on 13, 29, and 30 June 1994. Background cloud droplet sizes were relatively large on 13 and 29 June, while relatively small droplets were present on 30 June. Choosing the preferred MAS near-infrared channel for the size retrieval depends to some extent on the application. With marine stratocumulus clouds typically having increases in both droplet size and liquid water with height, no single value of effective radius is useful for all needs. For example, none of the channels can always provide an accurate liquid water path which is approximated from the retrievals as LWP $\approx \frac{2}{3}\tau r_e$ (r_e in micrometers) but is actually a vertical integration of that product. The accuracy of the approximation depends on cloud optical thickness, droplet size profile, and wavelength. A 2.1-μm retrieval, with its deeper penetration into the cloud, might be expected to provide better estimates than a 3.7-μm retrieval.

To explore this issue, calculations of liquid water path inferred from theoretical retrievals were made. Several combinations of thickness and size profiles, based on MAST retrievals in and out of ship tracks, were considered. On average, liquid water path estimates using 2.1-μm retrievals were within 8% of the exact value, about half the error in using 3.7-μm retrievals. More important, if liquid water path is unchanged in the development of a ship track, then it is desirable that differences in background cloud and in-track liquid water path retrievals should be minimized despite the optical thickness and size changes. Using 2.1-μm retrievals, this difference was not more than $\pm 5\%$ for several modeled profiles considered. For 3.7-μm retrievals, the difference errors are $+1\%$ to -7% relative to the exact value. This difference assumes no error in the retrieval of either optical thickness or effective radius and is a consequence of the estimation being based on a vertically homogeneous cloud. To consider the consequence of retrieval errors on liquid water path differences, we can write the ratio of the estimated liquid water path in the ship track to that outside the track as $\mathrm{LWP}_{\mathrm{in}}/\mathrm{LWP}_{\mathrm{out}} = (r_{e_{\mathrm{in}}}/r_{e_{\mathrm{out}}})(\tau_{\mathrm{in}}/\tau_{\mathrm{out}})$. Since ratios between size retrievals and the in situ measurements were found to be relatively constant, retrievals of $\mathrm{LWP}_{\mathrm{in}}/\mathrm{LWP}_{\mathrm{out}}$ should also be relatively correct, assuming the in situ measurements are relatively accurate and that there is no bias in the optical thickness retrievals. Optical thickness uncertainties have been discussed by Pincus et al. (1995) and Platnick and Valero (1995).

The 2.1-μm cloud retrievals are shown in this section because of their general agreement with FSSP effective radius measurements and the likelihood of being more representative of the vertically integrated liquid water path. The 1.6-μm channel may also be useful for this purpose, though its solution is more sensitive to the optical thickness retrieval (see Fig. 1).

Figure 6 shows retrievals for the southern portion of the ship track produced by the diesel-powered *Star Livorno* on 29 June 1994, which formed in a clean boundary layer (Hobbs et al. 2000). The MAS image shows a surprisingly complex scene at this high spatial resolution. The images cover an area of about 35 km along an instrument scan line (horizontal dimension on the figure) by 70 km in the vertical; pixels have not been spatially resampled across the scan line. The track width is about 7 km at the center of the images. The background has relatively large and highly variable droplet sizes, and a roll-cloud structure with some clear areas. In situ microphysical measurements by the University of Washington C-131A showed similar variability. Retrieved in-track effective radii are smaller than background sizes by about 5 μm or more. Background cloud optical thickness is also quite variable and might be partially responsible for obscuring the track in the optical thickness retrieval (cf. Fig. 3). However, there are many small-scale locations where a substantial decrease in droplet size corresponds to no significant change in the optical thickness. Since ship track optical thickness does not obviously change with respect to nearby background thicknesses, liquid water path merely follows the reduction in droplet sizes seen in the effective radius retrievals.

Figure 7 shows an unidentified ship track that formed on 30 June 1994 in a relatively uniform, thick, background cloud with small droplet sizes. The imaged region is about 35 km in the horizontal dimension by 40 km in the vertical. The track was seen in several adjacent ER-2 flight legs and is about 9 km wide. Retrieved in-track effective radii show a fair amount of structure along the edges, but with well-defined minima. Both background and in-track optical thicknesses are large and variable making it difficult to determine whether the two regions show significant differences. The variability seen in Figs. 6 and 7 suggests that track statistics derived from aircraft or surface ships could easily be biased by insufficient sampling.

Figure 8 summarizes MAS retrievals with histograms

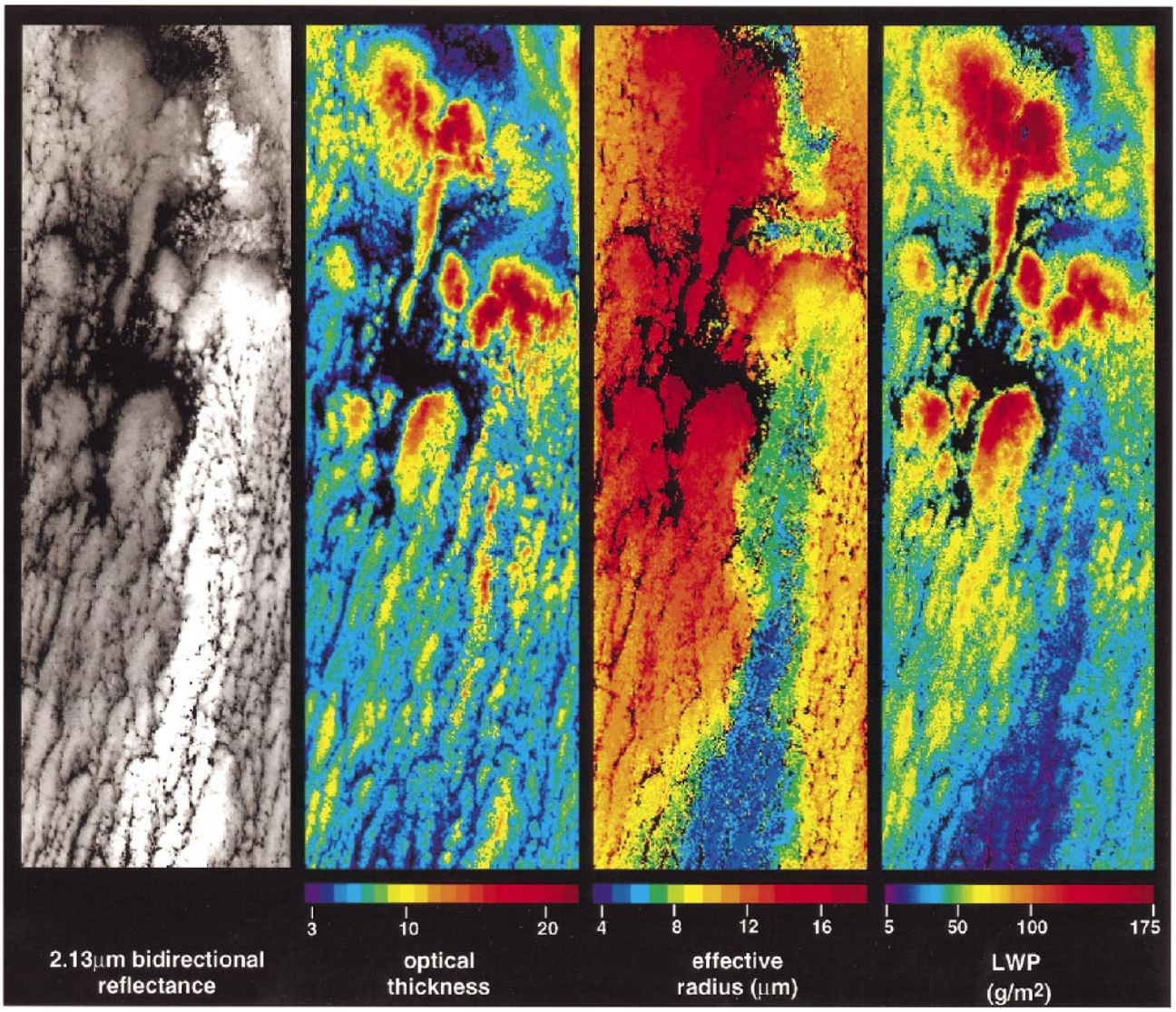

FIG. 6. Cloud reflectance and retrievals for the southern portion of the *Star Livorno* ship track (center of images at 35.95°N, 125.45°W) at 2000 UTC on 29 Jun 1994, using the MODIS Airborne Simulator visible and 2.13-μm channels. Each panel is 70 km long and 35 km wide.

for selected regions of Figs. 6 and 7 and several locations along the unknown ship track of 13 June 1994 (identified as a container ship in RC-10 photography, see Fig. 3). Droplet size reductions are significant in all cases, while optical thickness increases are small and generally within the background cloud variability (with the possible exception of the 13 June track).

In section 4, ship track contrast and susceptibility are derived with the more sensitive MAS 3.7-μm channel. Model estimates of the 3.7-μm reflectance based on shorter wavelength retrievals or in situ droplet sizes should be avoided if possible, especially if error in the physical theory or cloud model is a component of the 3.7-μm retrieval discrepancy. For this reason, both 3.7-μm track contrast and susceptibility calculations use MAS 3.7-μm retrievals. Unfortunately, in this channel high sun angles caused enhanced glory reflectances to cover large parts of the imaged clouds on most days. In these glory regions, significant changes in reflectance can occur over a small range of scan angles as details of the scattering phase function are seen in single scattered photons in backscattered directions (Spinhirne and Nakajima 1994). The default reflectance and emittance libraries used in the retrievals were calculated with an adding/doubling code (Twomey et al. 1966) with angular intervals equivalent to $\Delta\mu = 0.1$ for both solar and satellite zenith angles. The angular resolution needed in the libraries to account for glory directions at all possible scattering geometries would result in much larger libraries where resolution on the order of several

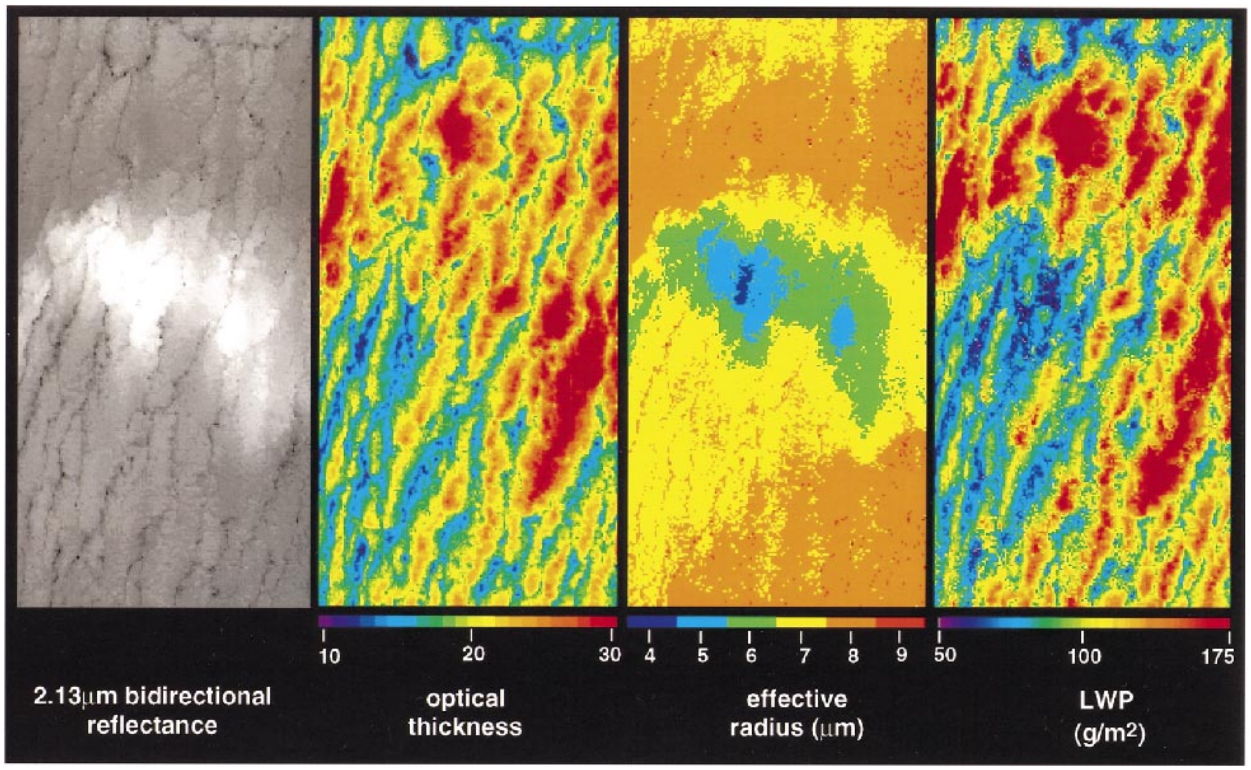

FIG. 7. Cloud reflectance and retrievals of an unidentified ship track at 2015 UTC on 30 Jun 1994, using the MODIS Airborne Simulator visible and 2.13-μm channels. Center of images located at 35.36°N, 125.13°W. Each panel is 40 km long and 35 km wide.

degrees would be required. Normally, these glory viewing angles could be avoided in the 3.7-μm retrievals. When glory directions could not be avoided, a modified reflectance library with the single scattering component removed was utilized. Then the phase function, using precise scattering angles, was used to calculate the exact single scattering component of reflectance and added to the modified library values. This use of the phase function resulted in retrieved droplet sizes being 10%–15% larger in glory regions.

b. AVHRR retrievals

Multiple tracks, extending over large regions, were found on 12, 13, 14, 27, 28, and 29 June 1994 in *NOAA-12* imagery collected at the Naval Postgraduate School in Monterey, California. For these six days, more than 18 000 pairs of in-track and nearby background cloud samples were collected from a total of about 110 tracks. Histograms of changes in cloud parameters for the pairs are shown in Fig. 9 for two of the days. As with the MAS retrievals, droplet size changes are the most obvious, while, on average, optical thickness is only slightly increased in tracks. Liquid water path is quite variable with average changes showing a small to insignificant decrease in tracks (see Fig. 9). In addition, the AVHRR retrievals gave significantly higher occurrences of large droplets ($>$15–20 μm) than did MAS 3.7-μm retrievals. With larger pixel sizes, it is possible that these retrievals suffer from inclusion of pixels that are not completely cloud filled. The issue of cloud fraction in these 1-km pixels is of critical importance. Calculations suggest that cloud-filled fractions of 0.7, for example, could increase retrieved effective radii by 4–6 μm over actual values, while retrieved optical thicknesses would decrease. It is not clear whether cloud fraction would be different between track and background regions. Because optical thickness was highly variable, cloud discrimination using an infrared channel was attempted. Pixels were screened by averaging over small areas, and only those with brightness temperatures below some specified threshold were included in the samples. However, this did not significantly affect the results. The AVHRR observed clouds in the morning, and so differences with midday MAS retrievals could also be due to diurnal changes (Minnis et al. 1992) or biases with solar zenith angle.

c. Comparison with previous studies

There are few pre-MAST ship track data with which to compare these retrievals. The in situ measurements of Radke et al. (1989) and King et al. (1993) showed increases in liquid water content and small reductions

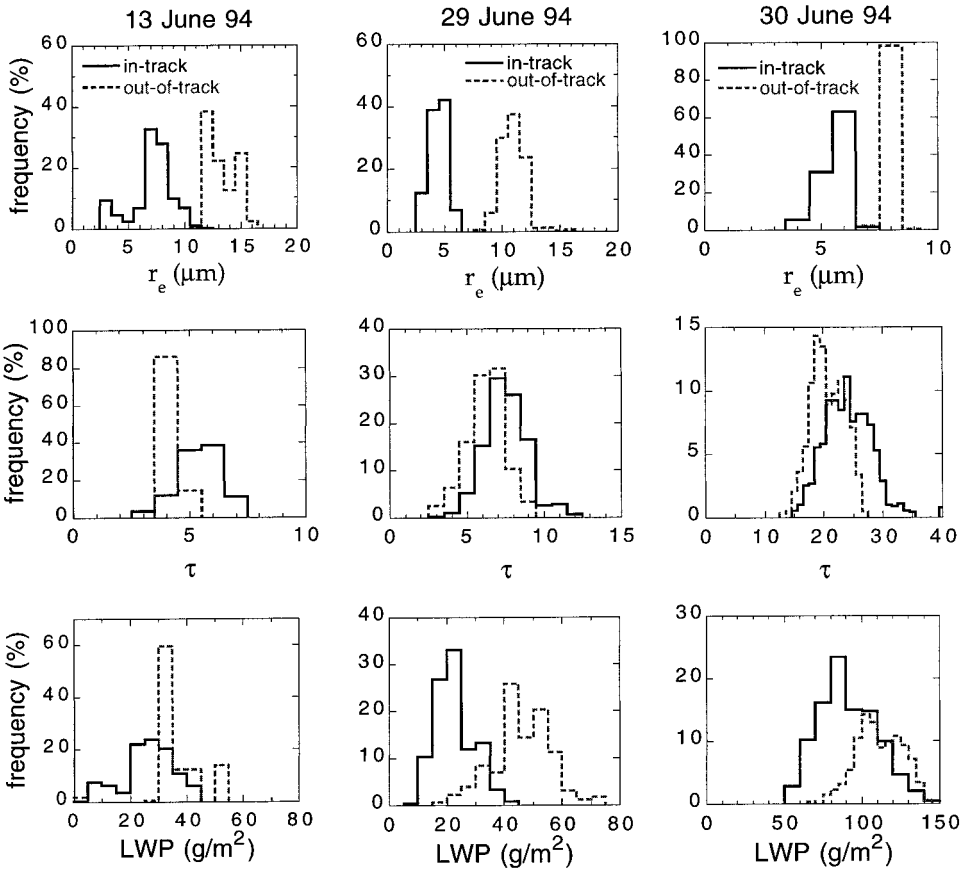

FIG. 8. Selected histograms of cloud retrievals using the MODIS Airborne Simulator visible and 2.13-μm channels, for three ship tracks from three different days. Retrievals are for selected track (solid lines) and nearby background cloud locations (dashed lines). Because of the large variability in both in-track and background cloud parameters, there is no unique histogram for any of the tracks.

in effective radius (<1 μm) in the two tracks they sampled. These ship tracks of Radke et al. were retrieved by Nakajima and Nakajima (1995) and Platnick and Twomey (1994) using the AVHRR. In both retrievals, size changes were minimal and liquid water path increased in the tracks. Other AVHRR ship track retrievals by Platnick and Twomey showed mostly increases in liquid water path for a small sample of tracks on a single day in a region off the coast of Washington State where effective radius reductions were significant. Measurements in two ship tracks off the Washington coast by Ferek et al. (1998) showed that drizzle was suppressed in the tracks compared to the ambient cloud. Ferek et al. (2000) investigated liquid water content modification in ship tracks during MAST and found that track liquid water content, though quite variable, did not significantly differ on average from background cloud amounts due to the relatively small amounts of liquid water contained in drizzle-sized drops in the clouds that were studied. The retrievals of this study suggest that average increases in track optical thickness are often on the order of the background cloud variability, though droplet size changes are obvious and can be quite large. Since liquid water path is approximated from the product of optical thickness and droplet size, estimates of track liquid water show a tendency to follow the lead of the more significant size changes and decrease relative to background values. The more fundamental issue raised by the liquid water retrievals, especially for the limited number of high resolution MAS retrievals, is the lack of significant optical thickness modification found in many of these tracks.

4. Background microphysics as a predictor of ship tracks

A summary of all AVHRR retrievals plotted as ship track contrast versus contrast susceptibility is shown in Fig. 10. Averages for individual tracks are also shown. With the exception of data from 12 June 1994, the largest relative increases in track reflectance correspond to larger susceptibilities. However, the great variability seen in all plots makes this relation less than definitive.

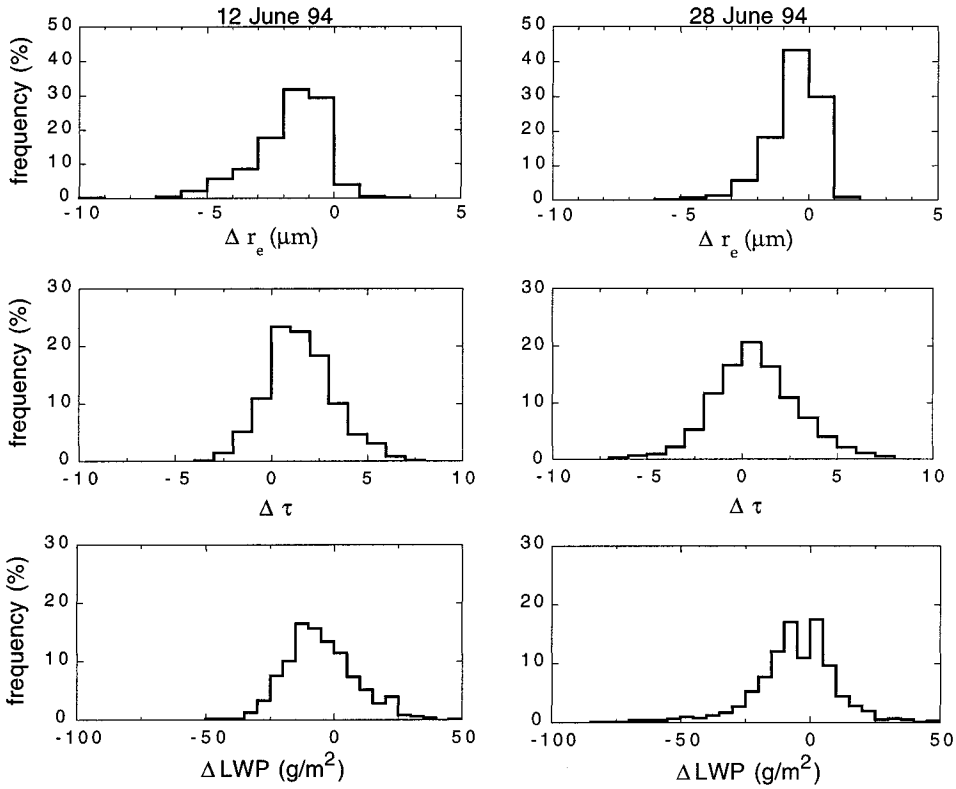

FIG. 9. Histograms of changes in AVHRR cloud retrievals (ship track minus background cloud) for 12 and 28 Jun 1994, calculated for numerous pairs of ship track and nearby background cloud locations.

Track-averaged points (triangles in Fig. 10) also show this variability.

Figure 11 shows a similar summary for MAS retrievals, which includes the three tracks discussed in the previous section. The figure uses retrievals compiled for the regions displayed in the histograms of Fig. 8. Three additional tracks from 13 June 1994 are plotted along with retrievals from 11 June 1994, a day of relatively uniform stratus in which no tracks were observed in the MAS imagery. Average values indicate a good correlation between track contrast and the 3.7-μm contrast susceptibility. The standard deviations for these points, indicated by the bars, are seen to be fairly large. The deviation in the calculated contrast susceptibility is caused by variability in the retrieved effective radii of the background cloud. It increases for the larger susceptibilities because of the radius-cubed dependence. The standard deviation in track contrast is also affected by the size retrievals since droplet absorption, and therefore cloud reflectance and emission, vary with effective radius. For example, given the same measured 3.7-μm radiance, a larger droplet size retrieval would imply a larger cloud emission component and a smaller cloud reflectance. This deviation depends on both background and in-track size variability. The standard deviations may have important implications to sampling size. If variations from the average values on the plot are not random from pixel to pixel but indicate actual cloud variability, which might exist on several scales, then large sampling sizes would be needed to give appropriate averages. For example, aircraft or ship measurements at limited locations in these track regions might only expect to be sampling somewhere within the standard deviation bars. The variability seen in the MAS retrievals of Figs. 6 and 7 makes these sampling concerns evident.

It was shown in the last section that 3.7-μm MAS effective radius retrievals are larger than in situ FSSP measurements by an average of 30%, for selected clouds imaged during coordinated flights between the ER-2 and C-131A. We now look at the effect of this size difference on the location of points in Fig. 11, for both susceptibility (abscissa) and track contrast (ordinate). Retrieval differences can be largely attributed to either measurement error (i.e., MAS or FSSP), or the cloud radiative model used in the retrievals. If the radiative model is inexact, then susceptibility calculations, which use the same model, would be suspect. This is also true for cloud reflectance estimates which directly depend on effective radius retrievals. Model error cannot be accounted for in susceptibility and track contrast calculations without knowing the source of the error. Of course, if FSSP in situ measurement error is the culprit, then MAS retrievals and subsequent calculations can

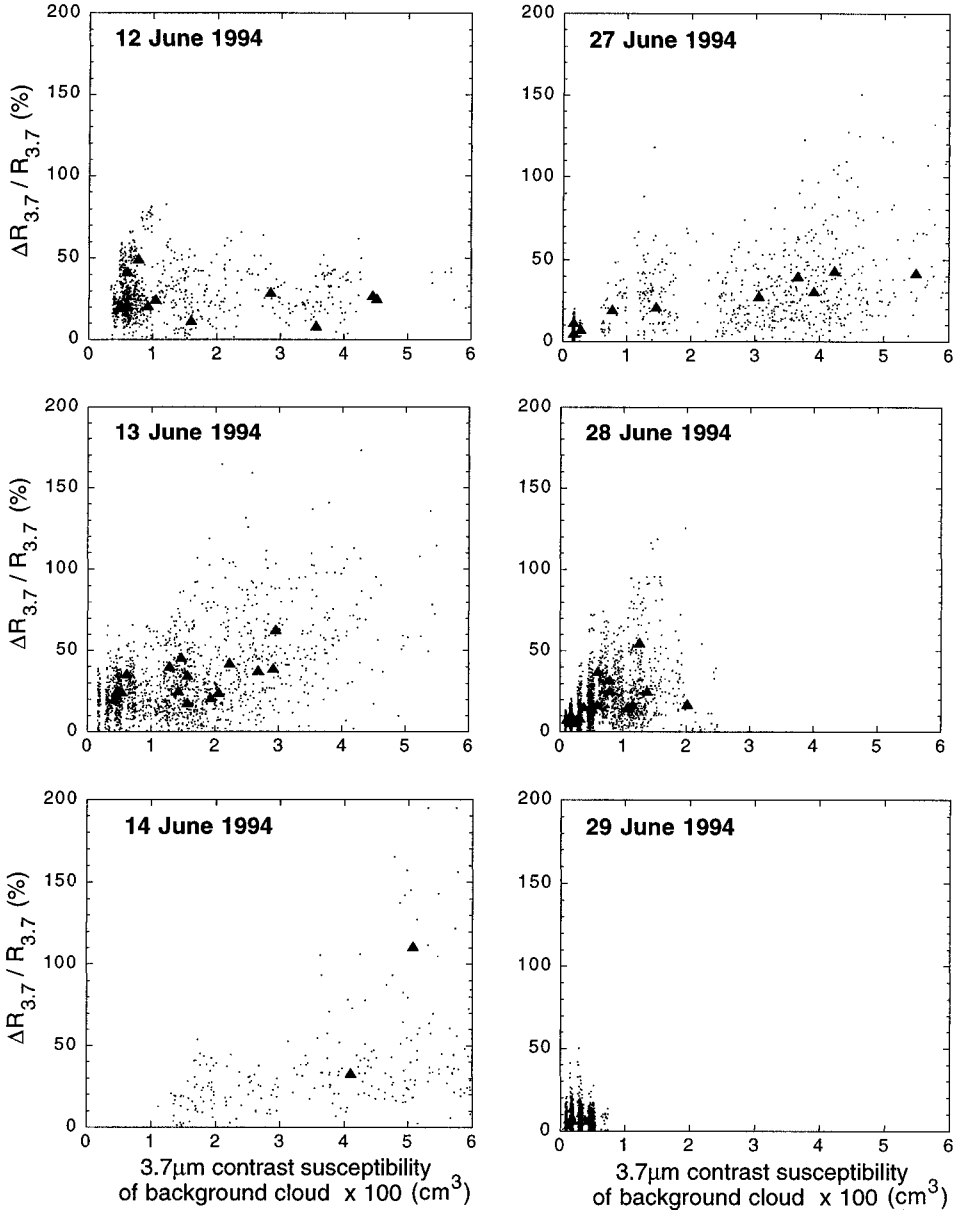

FIG. 10. Scatterplot of the measured relative change in the AVHRR 3.7-μm reflectance vs the calculated 3.7-μm contrast susceptibility of the background cloud, determined for numerous pairs of ship track and nearby background cloud locations. The averages for individual tracks are indicated by the triangles.

still be valid. Alternatively, if MAS measurement error is assumed responsible for the retrieval differences, then radiative calculations using FSSP measured droplet sizes would be valid.

The consequence of MAS measurement error can be determined from previous results. Since $r_{e_{\text{in situ}}}/r_{e_{\text{retrieved}}}$ was found to be approximately constant across the range of retrieved sizes, droplet sizes that would have been measured in situ by the FSSP can be inferred directly from MAS retrievals. The approximation of Eq. (5) indicates that the ratio of an in situ calculation of contrast susceptibility to one determined from a retrieved value would vary as $s_{\text{in situ}}/s_{\text{retrieved}} = (r_{e_{\text{in situ}}}/r_{e_{\text{retrieved}}})^3$, where s is susceptibility. With a 30% overestimation in the 3.7-μm retrieval size, $s_{\text{in situ}}/s_{\text{retrieved}}$ would be about 0.5. That is, if in situ size measurements are considered correct, the actual susceptibility would be half of the retrieved calculation, regardless of the retrieved size, and points on Fig. 11 would move to the left. Because cloud reflectance in a 3.7-μm band depends on droplet size, errors in retrieved sizes can also affect the determination of track contrast. If reflectance varies approximately as a power of effective radius (see section 2), we can write $R_{\text{in situ}}/R_{\text{retrieved}} = (r_{e_{\text{in situ}}}/r_{e_{\text{retrieved}}})^a$, where a is a constant.

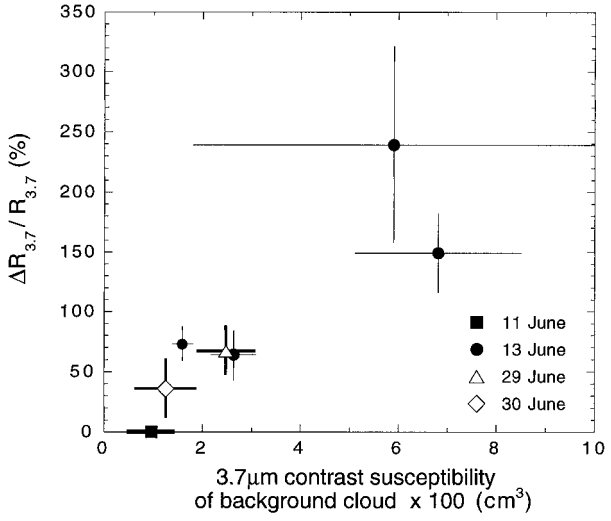

FIG. 11. Plot of the measured relative change in the MAS 3.7-μm channel reflectance vs the 3.7-μm contrast susceptibility of the background cloud on four different days. Each symbol represents the averages for a single ship track (except 11 Jun when no ship tracks were observed), while bars represent the standard deviations.

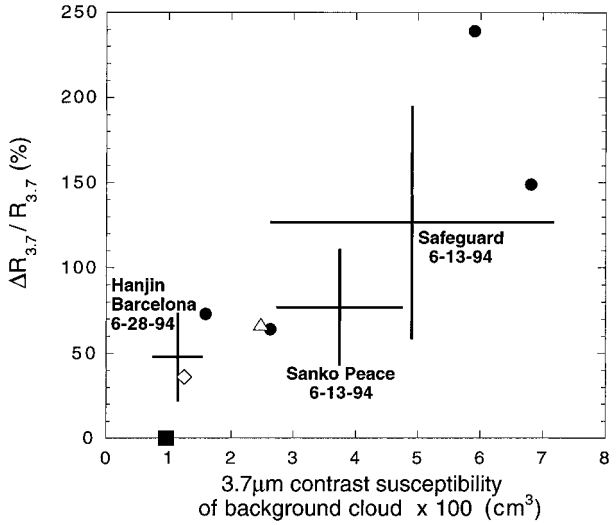

FIG. 12. Plot of the calculated relative change in a 3.7-μm channel reflectance vs the 3.7-μm contrast susceptibility of the background cloud for three ship tracks. Calculations based on in situ droplet size and above-cloud reflectance measurements of optical thickness made by the U.K. Meteorological Research Flight C-130 aircraft; bars represent the standard deviations. Averaged values for the MAS/ER-2 tracks of Fig. 11, with the same symbol definitions, are also shown.

Then for a constant overestimation in retrieved effective radius, $R_{\text{in situ}}/R_{\text{retrieved}}$ is also constant and so track contrast is unaffected. Therefore, to the extent that the power law approximation is valid, retrieved size errors due to MAS measurement errors would not appear to significantly affect the inference of ship track contrast.

If the average cloud liquid water content is known, a set of curves similar to Fig. 5a can be overlaid on Fig. 11 to test the agreement to which observed contrast and susceptibility is consistent with droplet increases (ΔN). University of Washington C-131A in situ measurements of liquid water content on 29 and 30 June 1994 were used to create such a set of curves. Since susceptibility results have been calculated for a nominal liquid water content of 0.3 g m^{-3}, the abscissa of Fig. 5a must be scaled by $0.3/W_{\text{meas}}$, where W_{meas} is the measured liquid water content at some representative vertical level, before a comparison can be made. The locations of the 29 and 30 June averages imply droplet increases of about 40 cm^{-3} for either day, while the C-131A measured increases of roughly 150 cm^{-3} on both days. If FSSP droplet size measurements are assumed correct, this lack of consistency might be partially attributed to 3.7-μm size retrievals being larger than in situ values. As just discussed, susceptibility would then decrease by about 50% and track contrast would be unchanged. The decrease in susceptibility would imply larger droplet increases (see Fig. 5), of about 100 cm^{-3} for these days, in closer agreement with in situ measurements.

The U.K. Meteorological Research Flight C-130 aircraft made in situ cloud microphysical measurements and above-cloud reflectance measurements during MAST. Effective droplet radius, derived from combined FSSP and 2-DC droplet spectra [see Martin et al. (1994) for instrument descriptions] and optical thickness derived from Multi-Channel Radiometer (Rawlins and Foot 1990) reflectance measurements, were used to calculate expected track contrast and contrast susceptibility for three identified tracks on 13 and 28 June 1994. Results of these calculations are plotted in Fig. 12 with the name of the ships indicated (the *Sanko Peace, Safeguard,* and *Hanjin Barcelona*). Standard deviations for the calculations were derived from measured standard deviations based on flight legs of about 40–100 km in length in the background cloud, and 6–80 km in the tracks. Average values for the MAS retrievals of Fig. 11 are also shown.

A good correlation exists between the relative change in the 3.7-μm reflectance and the contrast susceptibility of the background cloud when using average results from the combined datasets of Fig. 12. The correlation suggests that reasonable predictions of track contrast could have been made in these instances from knowledge of the background cloud microphysics (i.e., contrast susceptibility) alone, without regard to actual changes in cloud droplet numbers or the dynamics of the track formation. However, AVHRR results show more scatter than MAS retrievals perhaps indicating problems from undersampling background and in-track clouds. It may also be that the increased number of tracks analyzed in the AVHRR samples gives a truer indication of track variability. Cloud fraction effects at the lower image resolution are also a concern. Finally, AVHRR tracks are imaged in the morning in contrast to midday MAS images and so could differ due to di-

urnal changes. Liquid water content was set to 0.3 g m^{-3} in all susceptibility calculations; random deviations from this value would decrease the correlations.

5. Summary

The relative increase in ship track reflectance, compared to background cloud reflectance values, is a measure of track contrast. The derivative of contrast with respect to cloud droplet concentration is a modified form of the cloud susceptibility parameter (Twomey 1991) and has been termed the ''contrast susceptibility.'' This sensitivity parameter increases with wavelength into the near-infrared as less droplet absorption, due to smaller in-track cloud droplets, results in larger relative reflectance increases than for a visible channel responding only to larger in-track optical thickness. The 3.7-μm band has the largest sensitivity to droplet numbers among the channels typically used for cloud remote sensing and is expected to have a factor of 2–6 times greater sensitivity than visible channels.

Both MAS and AVHRR retrievals show great variability in both background cloud and ship track optical thickness and effective radius. Generally speaking, retrievals for our dataset show that effective radius reduction is the most apparent signature of ship tracks; optical thickness changes in tracks are not much larger, on average, than background variability; and the inferred liquid water path, following the lead of droplet size changes, decreases in tracks more often than not. The variability seen in high-resolution MAS imagery indicates that it may often be difficult for situ aircraft and surface-based instruments to obtain the sufficient spatial sampling necessary for inferring ship track statistics.

This paper has focused on stratocumulus clouds in which ship tracks were readily observed. Less attention has been given to the meaning and use of cloud susceptibility on days when no tracks form. We have seen that once a track forms, its contrast is reasonably correlated with the contrast susceptibility of the background cloud. But we have not discussed whether susceptibility is an important precursor for the existence of tracks. Coakley et al. (2000) discuss this issue with regard to cloud boundary layer decoupling. Further, we have not looked at the variability of effluent emitted by ships and the ability of the resulting aerosol particle sizes to serve as cloud condensation nuclei (Hobbs et al. 2000; Frick and Hoppel 2000).

Correlations between the 3.7-μm track contrast and the background cloud 3.7-μm contrast susceptibility are reasonably good for averaged MAS retrievals and C130 in situ measurements (Fig. 12). If this observed correlation is generally true, estimates of potential ship track formation from background cloud microphysics would be possible without needed details of ship effluent, droplet nucleation, and dynamic processes (given that boundary layer dynamics and ship effluent are suitable for track development). However, AVHRR retrievals show more scatter and poorer correlations.

Acknowledgments. We are grateful to D. Babb and W. Syrett for soundings launched from the *Glorita*; J. A. Coakley for helpful discussions; T. Nakajima, R. Pincus, M. Wang, and two anonymous reviewers for their helpful comments; D. P. Kratz for use of his *k* distributions; and G. T. Arnold, M. Fitzgerald, P. S. Grant, J. S. Myers, and L. E. Gumley for calibration and MAS deployment support.

REFERENCES

Arnold, G. T., and Coauthors, 1996: MODIS Airborne Simulator radiometric calibration. *SPIE Proc.*, **2820,** 56–66.

Baumgardner, D., 1982: A description of FSSP auxiliary variables and their use. NCAR Tech. Note 199, 103 pp.

Bohren, C. F., 1987: Multiple scattering of light and some of its observable consequences. *Amer. J. Phys.*, **55,** 524–533.

Charlson, R. J., S. E. Schwartz, J. M. Hales, R. D. Cess, J. A. Coakley Jr., J. E. Hansen, and D. J. Hofmann, 1992: Climate forcing by anthropogenic aerosols. *Science*, **255,** 423–430.

Coakley, J. A., Jr., R. L. Bernstein, and P. A. Durkee, 1987: Effect of ship-stack effluents on cloud reflectivity. *Science*, **237,** 1020–1022.

——, and Coauthors, 2000: The appearance and disappearance of ship tracks on large spatial scales. *J. Atmos. Sci.*, **57,** 2765–2778.

Conover, J. H., 1966: Anomalous cloud lines. *J. Atmos. Sci.*, **23,** 778–785.

——, 1969: New observations on anomalous cloud lines. *J. Atmos. Sci.*, **26,** 1153–1154.

Ferek, R. J., D. A. Hegg, P. V. Hobbs, P. Durkee, and K. Nielsen, 1998: Measurements of ship-induced tracks in clouds off the Washington coast. *J. Geophys. Res.*, **103,** 23 199–23 206.

——, and Coauthors, 2000: Drizzle suppression in ship tracks. *J. Atmos. Sci.*, **57,** 2707–2728.

Frick, G. M., and W. A. Hoppel, 2000: Airship measurements of ship's exhaust plumes and their effect on marine boundary layer clouds. *J. Atmos. Sci.*, **57,** 2625–2648.

Garrett, T. J., and P. V. Hobbs, 1995: Long-range transport of continental aerosols over the Atlantic Ocean and their effects on cloud structure. *J. Atmos. Sci.*, **52,** 2977–2984.

Gerber, H., B. G. Arends, and A. S. Ackerman, 1994: New microphysics sensor for aircraft use. *Atmos. Res.*, **31,** 235–252.

Han, Q., W. Rossow, R. Welch, A. White, and J. Chou, 1995: Validation of satellite retrievals of cloud microphysics and liquid water path using observations from FIRE. *J. Atmos. Sci.*, **52,** 4183–4195.

Hobbs, P. V., and Coauthors, 2000: Emissions from ships with respect to their effects on clouds. *J. Atmos. Sci.*, **57,** 2570–2590.

King, M. D., L. F. Radke, and P. V. Hobbs, 1993: Optical properties of marine stratocumulus clouds modified by ships. *J. Geophys. Res.*, **98,** 2729–2739.

——, and Coauthors, 1996: Airborne scanning spectrometer for remote sensing of cloud, aerosol, water vapor, and surface properties. *J. Atmos. Oceanic Technol.*, **13,** 777–794.

Knollenberg, R. G., 1981: Techniques for probing cloud microstructure. *Clouds: Their Formation, Optical Properties, and Effects*, P. V. Hobbs and A. Deepak, Eds., Academic Press, 15–91.

Kratz, D. P., 1995: The correlated k-distribution technique as applied to the AVHRR channels. *J. Quant. Spectrosc. Radiat. Transfer*, **53,** 501–517.

Martin, G. M., D. W. Johnson, and A. Spice, 1994: The measurement and parameterization of the effective radius of warm stratocumulus clouds. *J. Atmos. Sci.*, **51,** 1823–1842.

Minnis, P., P. W. Heck, D. F. Young, C. W. Fairall, and J. B. Snider,

1992: Stratocumulus cloud properties derived from simultaneous satellite and island-based instrumentation during FIRE. *J. Appl. Meteor.*, **31,** 317–339.

Moeller, C. C., P. S. Grant, D. D. LaPorte, L. E. Gumley, P. Hajek, W. P. Menzel, J. S. Myers, and S. White, 1996: Blackbody emissivity considerations for radiometric calibration of the MODIS Airborne Simulator (MAS) thermal channels. *SPIE Proc.*, **2820,** 44–55.

Mossop, S. C., 1983: Intercomparison of instruments used for measurement of cloud drop concentration and size distribution. *J. Climate Appl. Meteor.*, **22,** 419–428.

Nakajima, T., and M. D. King, 1990: Determination of the optical thickness and effective particle radius of clouds from reflected solar radiation measurements. Part I: Theory. *J. Atmos. Sci.*, **47,** 1878–1893.

——, ——, J. D. Spinhirne, and L. F. Radke, 1991: Determination of the optical thickness and effective particle radius of clouds from reflected solar radiation measurements. Part II: Marine stratocumulus observations. *J. Atmos. Sci.*, **48,** 728–750.

Nakajima, T. Y., and T. Nakajima, 1995: Wide-area determination of cloud microphysical properties from NOAA AVHRR measurements for FIRE and ASTEX regions. *J. Atmos. Sci.*, **52,** 4043–4059.

Noonkester, V. R., 1984: Droplet spectra observed in marine stratus cloud layers. *J. Atmos. Sci.*, **41,** 829–845.

Pincus, R., M. Szczodrak, J. Gu, and P. Austin, 1995: Uncertainty in cloud optical depth estimates made from satellite radiance measurements. *J. Climate*, **8,** 1453–1462.

Platnick, S., 1997: The scales of photon transport in cloud remote sensing problems. *IRS '96: Current Problems in Atmospheric Radiation*, W. L. Smith and K. Stamnes, Eds., A. Deepak, 206–209.

——, and S. Twomey, 1994: Determining the susceptibility of cloud albedo to changes in droplet concentration with the Advanced Very High Resolution Radiometer. *J. Appl. Meteor.*, **33,** 334–347.

——, and F. P. J. Valero, 1995: A validation of a satellite cloud retrieval during ASTEX. *J. Atmos. Sci.*, **52,** 2985–3001.

Radke, L. F., J. A. Coakley Jr., and M. D. King, 1989: Direct and remote sensing observations of the effects of ships on clouds. *Science*, **246,** 1146–1149.

Rawlins, F., and J. S. Foot, 1990: Remotely sensed measurements of stratocumulus properties during FIRE using the C130 aircraft multichannel radiometer. *J. Atmos. Sci.*, **47,** 2488–2503.

Scorer, R. S., 1987: Ship trails. *Atmos. Environ.*, **21,** 1417–1425.

Spinhirne, J. D., and T. Nakajima, 1994: The glory of clouds in the near infrared. *Appl. Opt.*, **33,** 4652–4662.

Stephens, G. L., and S. Tsay, 1990: On the cloud absorption anomaly. *Quart. J. Roy. Meteor. Soc.*, **116,** 671–704.

Syrett, W. J., 1994: Low-level temperature and moisture structures from MAST: 5–29 June 1994. Pennsylvania State University Department of Meteorology Rep., 35 pp. [Available from Department of Meteorology, 503 Walker Building, The Pennsylvania State University, University Park, PA 16802.]

Taylor, J. P., and A. McHaffie, 1994: Measurements of cloud susceptibility. *J. Atmos. Sci.*, **51,** 1298–1306.

Twomey, S., 1974: Pollution and the planetary albedo. *Atmos. Environ.*, **8,** 1251–1256.

——, 1977: The influence of pollution on the shortwave albedo of clouds. *J. Atmos. Sci.*, **34,** 1149–1152.

——, 1991: Aerosols, clouds and radiation. *Atmos. Environ.*, **254,** 2435–2442.

——, and C. F. Bohren, 1980: Simple approximations for calculations of absorption in clouds. *J. Atmos. Sci.*, **37,** 2086–2094.

——, and T. Cocks, 1989: Remote sensing of cloud parameters from spectral reflectance in the near-infrared. *Beitr. Phys. Atmos.*, **62,** 172–179.

——, H. Jacobowitz, and H. B. Howell, 1966: Matrix methods for multiple scattering problems. *J. Atmos. Sci.*, **23,** 101–108.

——, H. B. Howell, and T. A. Wojciechowski, 1968: Comments on ''Anomalous cloud lines.'' *J. Atmos. Sci.*, **25,** 333–334.